Propagation of elastic waves in a fluid-loaded anisotropic functionally graded waveguide: Application to ultrasound characterization

Cécile Baron, Salah Naili

Propagation of elastic waves in a fluid-loaded anisotropic functionally graded waveguide: Application to ultrasound characterization

Cécile Baron and Salah Naili[a)]
Laboratoire de Mécanique Physique, Faculté des Sciences et Technologie, Université Paris 12–Val de Marne, 61 Avenue du Général de Gaulle, 94010 Créteil Cedex, France

(Received 27 June 2008; revised 19 August 2009; accepted 22 December 2009)

Non-destructive evaluation of heterogeneous materials is of major interest not only in industrial but also in biomedical fields. In this work, the studied structure is a three-layered one: A laterally heterogeneous anisotropic solid layer is sandwiched between two acoustic fluids. An original method is proposed to solve the wave equation in such a structure without using a multilayered model for the plate. This method is based on an analytical solution, the matricant, explicitly expressed under the Peano series expansion form. This approach is validated for the study of a fluid-loaded anisotropic and homogeneous plane waveguide with two different fluids on each side. Then, original results are given on the propagation of elastic waves in an asymmetrically fluid-loaded waveguide with laterally varying properties. This configuration notably corresponds to the axial transmission technique to the ultrasound characterization of cortical bone *in vivo*.
 [DOI: 10.1121/1.3292949]

PACS number(s): 43.40.Dx, 43.20.Mv [ADP] Pages: 1–XXXX

I. INTRODUCTION

A lot of natural media have unidirectional varying elastic properties. The mantel crust, the oceans, and cortical bone are some of these functionally graded media. Scientists focused on the advantages presented by this type of materials in terms of mechanical behavior, and since the 1980s, they developed industrial functionally graded materials (FGMs) particularly exploited in high-technology and biomedical applications. Consequently, the non-destructive evaluation of these materials is a key issue. Surface and guided waves play a major role in non-destructive testing and evaluation of complex structures. Several studies are dedicated to the leaky Lamb wave propagation in fluid-loaded plates (Chimenti and Nayfeh, 1990; Chimenti and Rokhlin, 1990; Deschamps and Poncelet, 2000). In all these studies, the media are homogeneous or multilayered. In this work, we introduce a general method to take into account the continuity of the property variation in an anisotropic waveguide. This method is based on the knowledge of an analytical solution of the wave equation, the matricant, explicitly expressed via the Peano series (Peano, 1888). The accuracy of the numerical evaluation of this solution and its validity domain are perfectly managed (Baron, 2005; Youssef and El-Arabawi, 2007). Because it deals with an analytical solution, all the wave propagation parameters are controlled. This represents an advantage with respect to numerical methods such as finite-element and finite-difference methods for which the problem treated is a global one, making difficult to analyze and interpret the experimental data, which result from the interaction and coupling of numerous physical phenomena. To the best of our knowledge, this is the first method to evaluate the mechanical behavior of a fluid-loaded anisotropic waveguide with continuously varying properties without modeling the FGM plate by a multilayered plate. Consequently, in the context of real materials with continuously varying properties (such as bone, bamboo, or manufactured FGM), this method could allow assessing the solution to a more realistic model with a controlled accuracy and without an increase in the computation-time.

In this work, we first present the method and its setup with fluid-structure interaction; then we proceed to the validation of the method by comparing our results to the dispersion curves obtained from classical schemes on homogeneous waveguides (isotropic and anisotropic). Two advantages of the method are underlined: (i) An asymmetric fluid-loading may be taken into account without modifying the scheme for the numerical solution, and (ii) the influence of the property gradient on the ultrasonic response of the waveguide may be investigated via the frequency spectrum of the reflection coefficient modulus. Finally, we get onto the relevancy of this model applied to the ultrasound characterization of cortical bone by the axial transmission technique.

II. BACKGROUND

Contemporary work efforts over the last 2 decades illustrate some of the technology interest on guided waves to non-destructive evaluation. Namely, Rose (2002) gave a review of ultrasonic guided wave inspection potential. A lot of papers deal with the interaction between guided waves and a solid plate immersed in a fluid or embedded between two different fluids. Guided modes in an infinite elastic isotropic plate in vacuum were first treated by Rayleigh (1885) then by Lamb (1917). The Lamb wave problem is reserved, strictly speaking, for wave propagation in a traction-free homogeneous isotropic plate. To deal with guided modes in a fluid-loaded plate, we use the term "leaky Lamb waves" as the energy is partly radiated in the fluids on both sides of the plate. For the basic Lamb problem—plate in vacuum—the

[a)]Author to whom correspondence should be addressed. Electronic mail: naili@univ-paris12.fr

solutions of the dispersion equation are real whereas in the case of a plate bounded by media on both sides, the dispersion equation has complex solutions. In 1961, Worlton (1961) gave an experimental confirmation of the theoretical work of Lamb (1917), by obtaining experimentally the dispersion curves of aluminum and zirconium plates, asserting that water loading has little effect on the behavior of waves in plates. In 1976, Pitts *et al.* (1976) presented some numerical test results on the relationship between real part of the reflection coefficient poles and the phase velocity of leaky Lamb modes in a homogeneous isotropic brass plate in water. Folds and Loggins (1977) proposed analytical expressions of the reflection and transmission coefficients for plane waves at oblique incidence on a multilayered isotropic plate immersed in water based on Brekhovskikh's (1980) analysis. They found good agreement with their theoretical results and experimental data. Few years later, Fiorito *et al.* (1979) developed a resonance formalism for the fluid-loaded elastic plate and gave some theoretical and numerical results for an isotropic steel plate immersed in the water. This formalism was generalized to the interactions of acoustic plane waves with an asymmetrically fluid-loaded elastic plate by Franklin *et al.* (2001). Nayfeh, Chimenti, and Rokhlin produced a lot of works on wave propagation in anisotropic media and particularly in fiber composite plates immersed in a fluid (Chimenti and Nayfeh, 1986, 1990; Chimenti and Rokhlin, 1990; Nayfeh and Chimenti, 1988, 1989; Rokhlin and Wang, 2002). Based on their formalism, Deschamps and Poncelet (2000) placed the emphasis on the difference between what they called transient Lamb wave-solutions of the characteristic equation of the plate for complex frequency and real slowness (time attenuation), and heterogeneous Lamb waves for which the slowness is complex and the frequency is real (spatial attenuation). These two ways of resolution of the dispersion equation have two different physical meanings—space or time attenuation—and consequences of this difference are developed in their paper (Deschamps and Poncelet, 2000). A critical point is the validity of the Cremer's coincidence hypothesis: The real couples (angular frequency ω and phase velocity v_φ), such that the reflection coefficient is minimum, may be identified as velocity dispersion of plate waves. Experimentally checked in a lot of configurations, it appears to be not well satisfied in several cases (for instance, graphite-epoxy plates when the ratio between fluid and plate mass densities is not "small") (Chimenti and Nayfeh, 1986; Nayfeh and Chimenti, 1988). The results obtained by Deschamps and Poncelet (2000) on fluid-loaded plate show a good correlation between dispersion curves obtained in complex frequency and the minima of the reflection coefficient, which suggests that the Cremer's coincidence principle is still valid considering time attenuation. All these studies show the evidence that the wave propagation in fluid-loaded elastic plate emerges as a very delicate problem, which needs cautious treatment.

III. GENERAL FORMULATION OF THE PROBLEM

We consider a three-dimensional multilayer system composed of one elastic solid layer sandwiched between two acoustic fluid layers. Let $\mathbf{R}(\mathrm{O},\mathbf{x}_1,\mathbf{x}_2,\mathbf{x}_3)$ be the Cartesian frame of reference where O is the origin of the space and $(\mathrm{x}_1,\mathrm{x}_2,\mathrm{x}_3)$ is an orthonormal basis for this space. The coordinate of the generic point $\mathbf{x}$ in $\mathbf{R}$ is specified by (x_1,x_2,x_3). The acoustic fluid layers occupy an open unbounded domain. Both fluids f_1 and f_2 are supposed perfect, of respective mass densities ρ_{f_1} and ρ_{f_2}; the constant speeds of sound in each fluid are c_{f_1} and c_{f_2}, respectively. The thickness of the solid layer is denoted by d and its mass density by ρ. The interfaces between the fluids and the solid layer are infinite planes parallel to the $(\mathbf{x}_1,\mathbf{x}_2)$-plane. The $\mathbf{x}_3$-axis is oriented downward and the origin O is located at the interface between the upper fluid f_1 and the solid layer. Therefore, we assume that the structure is a two-dimensional one and that the guided waves travel in the plane $x_2=0$; in the following parts, this coordinate is implicit and is omitted in the mathematical expressions. Moreover, the solid layer will be so-called plate.

The elastic plate is supposed to be anisotropic and is liable to present continuously varying properties along its thickness ($\mathbf{x}_3$-axis). These mechanical properties are represented by the stiffness fourth-order tensor $\mathbb{C}=\mathbb{C}(x_3)$ and the mass density $\rho=\rho(x_3)$.

A. System equations

1. The wave equation in the fluid f_n (for n=1 or 2)

In the fluid f_n and the context of the linear acoustic theory, the linearized Euler equation and the constitutive equations are written as

$$-\frac{\partial p^{(n)}}{\partial x_j}=\rho_{f_n}\frac{\partial^2 u_j^{(n)}}{\partial t^2},$$

$$p^{(n)}=K_{f_n}\,\mathrm{div}\,\mathbf{u}^{(\mathbf{n})}, \tag{1}$$

where $\mathbf{u}^{(n)}$ and $p^{(n)}$, respectively, represent the displacement vector and the pressure in the fluid f_n; its compressibility and the speed of sound in the fluid at equilibrium are, respectively, K_{f_n} and $c_{f_n}=\sqrt{K_{f_n}/\rho_{f_n}}$. The operator div is the divergence.

The solutions of system (1) for the fluid f_n are sought under the form

$$\mathbf{f}_n(x_1,x_2;t)=\mathbf{A}_n(x_3)\exp\,\imath(k_1x_1+k_3^{(n)}x_3-\omega t), \tag{2}$$

where k_1 and $k_3^{(n)}$ are the wavenumbers, respectively, along the $\mathbf{x}_1$-axis and $\mathbf{x}_3$-axis in the fluid f_n; the angular frequency is noted ω and $\imath$ is the imaginary unit.

We consider an incident wave reaching the plate at an angle θ_1 from the $\mathbf{x}_3$-axis in the fluid f_1. The incident displacement-field is defined in the following form, assuming that its amplitude is normalized:

$$\mathbf{u}_I^{(1)}=\begin{pmatrix}\sin\,\theta_1\\0\\\cos\,\theta_1\end{pmatrix}\exp\,\imath(k_1x_1+k_3^{(1)}x_3-\omega t), \tag{3}$$

with $k_1=(\omega/c_{f_1})\sin\,\theta_1$ and $k_3^{(1)}=(\omega/c_{f_1})\cos\,\theta_1$. From this, the expressions of the reflected displacement-field $\mathbf{u}_R^{(1)}$ in f_1 and of the transmitted displacement-field $\mathbf{u}_T^{(2)}$ in f_2 are deduced as follows:

$$\mathbf{u}_R^{(1)} = R\begin{pmatrix}\sin\theta_1\\0\\-\cos\theta_1\end{pmatrix}\exp\iota(k_1x_1 - k_3^{(1)}x_3 - \omega t),$$

$$\mathbf{u}_T^{(2)} = T\frac{c_{f_2}}{c_{f_1}}\begin{pmatrix}\sin\theta_1\\0\\\cos\theta_1\end{pmatrix}\exp\iota(k_1x_1 + k_3^{(2)}x_3 - \omega t). \quad (4)$$

where $R=R(x_1,x_3;t)$ and $T=T(x_1,x_3;t)$, respectively, represent the reflection and transmission coefficients, which will be expressed explicitly in the sequel. The incident, reflected, and transmitted pressure fields, respectively, noted $p_I^{(1)}$, $p_R^{(1)}$, and $p_T^{(2)}$, are deduced from expressions (3) and (4), and the second equation of the system (1)

$$p_I^{(1)} = -\iota\omega \times \rho_{f_1}c_{f_1} \times \exp\iota(k_1x_1 - k_3^{(1)}x_3 - \omega t),$$

$$p_R^{(1)} = -\iota\omega \times \rho_{f_1}c_{f_1} \times R \times \exp\iota(k_1x_1 - k_3^{(1)}x_3 - \omega t),$$

$$p_T^{(2)} = -\iota\omega \times \rho_{f_2}c_{f_2} \times T \times \exp\iota(k_1x_1 + k_3^{(2)}x_3 - \omega t). \quad (5)$$

B. The wave equation in the plate waveguide

The body forces in the solid plate are neglected. The balance equation of linear momentum associated with the constitutive law of linear elasticity (Hooke's law) gives the following equations:

$$\frac{\partial\sigma_{ij}}{\partial x_j} = \rho\frac{\partial^2 u_i}{\partial t^2},$$

$$\sigma_{ij} = \frac{1}{2}C_{ijk\ell}\left(\frac{\partial u_k}{\partial x_\ell} + \frac{\partial u_\ell}{\partial x_k}\right), \quad (6)$$

where u_i (for $i=1,\ldots,3$) and σ_{ij} (for $i,j=1,\ldots,3$), respectively, represent the components of the displacement-field $\mathbf{u}$ and of the stress $\boldsymbol{\sigma}$. In system (6), the Einstein convention of summation on repeated indices is used. The solutions are sought for the vectors of displacement $\mathbf{u}$ and traction σ_{i3} (for $i=1,\ldots,3$) (assumed to be harmonic in time t and space along the $\mathbf{x}_1$-axis) under the form

$$\mathbf{f}(x_1,x_3;t) = \mathbf{A}(x_3)\exp\iota(k_1x_1 - \omega t). \quad (7)$$

C. Fluid-loading interface conditions

The conditions at both interfaces $x_3=0$ and $x_3=d$ are the continuity of the normal displacement and the one of the normal stress. We consider that the fluids f_1 and f_2 are perfect; consequently, the shear stresses are zero at the interfaces $[\sigma_{13}(x_1,0;t)=\sigma_{13}(x_1,d;t)=0$ and $\sigma_{23}(x_1,0;t)=\sigma_{23}(x_1,d;t)=0]$. The following relations are obtained:

$$u_3(x_1,0;t) = u_3^{(1)}(x_1,0;t), \quad u_3(x_1,d;t) = u_3^{(2)}(x_1,d;t),$$

$$\sigma_{33}(x_1,0;t) = -p^{(1)}(x_1,0;t), \quad \sigma_{33}(x_1,d;t) = -p^{(2)}(x_1,d;t), \quad (8)$$

with

$$u_3^{(1)} = \mathbf{u}_I^{(1)}\cdot\mathbf{x}_3 + \mathbf{u}_R^{(1)}\cdot\mathbf{x}_3, \quad u_3^{(2)} = \mathbf{u}_T^{(2)}\cdot\mathbf{x}_3 \quad \text{and}$$

$$p^{(1)} = p_I^{(1)} + p_R^{(1)}, \quad p^{(2)} = p_T^{(1)}. \quad (9)$$

D. A closed-form solution: The matricant

Introducing expression (7) in Eq. (6), we obtain the wave equation under the form of a second-order differential equation with non-constant coefficients. For particular forms of profiles, this equation has analytical solutions expressed with special functions (Bessel or Hankel functions) (Vlasie and Rousseau, 2004). But, in the general case, there is no analytical solution to the problem thus formulated. The most current methods to solve the wave equation in unidirectionally heterogeneous media are derived from the Thomson–Haskell method (Haskell, 1953; Thomson, 1950). These methods are appropriate for multilayered media (Hosten and Castaings, 2003; Kenneth, 1982; Lévesque and Piché, 1992; Wang and Rokhlin, 2001). But, for continuously varying media, these techniques mean to replace the continuous profiles of properties with step-wise functions. Thereby, the studied problem becomes an approximate one, even before the resolution step; the accuracy of the solution as its validity domain is hard to evaluate. Moreover, the multilayered model of the waveguide creates some "virtual" interfaces likely to induce artifacts. In order to deal with the exact problem, that is to keep the continuity of the properties' variation, the wave equation is re-written under the form of an ordinary differential equation system with non-constant coefficients for which an analytical solution exists: the matricant (Baron, 2005).

1. Hamiltonian form of the wave equation

We consider that the plate presents material symmetries that allow decoupling the pressure–shear vertical (P-SV) waves, polarized in the propagation plane $(\mathbf{x}_1,\mathbf{x}_3)$ and the shear horizontal (SH) waves polarized along $\mathbf{x}_2$-axis. The incident medium f_1 is a perfect fluid; only the P-SV waves travel in the plate. Applying a spatio-temporal Fourier transform on (x_1,t) of the displacement-field [noted $\hat{\mathbf{u}}(k_1,x_3;\omega)$ after Fourier transform] and on the traction field [noted $\hat{\sigma}_{i3}(k_1,x_3;\omega)$ for $i=1,\ldots,3$] and using the Voigt notation ($C_{ijk\ell}$ for $i,j,k,\ell=1,\ldots,3$ is replaced with c_{IJ} for $I,J=1,\ldots,6$), Eq. (6) leads to Stroh's (1962) sextic plate formalism (Hamiltonian formulation of the wave equation)

$$\frac{\partial\hat{\sigma}_{13}}{\partial x_3} = \rho(\iota\omega)^2\hat{u}_1 - \iota k_1\hat{\sigma}_{11}, \quad \frac{\partial\hat{\sigma}_{33}}{\partial x_3} = \rho(\iota\omega)^2\hat{u}_3 - \iota k_1\hat{\sigma}_{13}, \quad (10)$$

$$\hat{\sigma}_{11} = \iota k_1 c_{11}\hat{u}_1 + c_{33}\frac{\partial\hat{u}_3}{\partial x_3}, \quad \hat{\sigma}_{13} = c_{55}\left(\frac{\partial\hat{u}_1}{\partial x_3} + \iota k_1\hat{u}_3\right),$$

$$\hat{\sigma}_{33} = \iota k_1 c_{13}\hat{u}_1 + c_{33}\frac{\partial\hat{u}_3}{\partial x_3}. \quad (11)$$

According to Eqs. (10) and (11), $\hat{\sigma}_{11}$ is function of $\hat{u}_1$ and $\hat{\sigma}_{33}$. The wave equation becomes a matrix system expressed using the Thomson–Haskell parametrization of Stroh's (1962) sextic plate formalism

$$\frac{d}{dx_3}\begin{pmatrix} \iota\omega\hat{u}_1 \\ \iota\omega\hat{u}_3 \\ \hat{\sigma}_{13} \\ \hat{\sigma}_{33} \end{pmatrix} = \iota\omega \begin{pmatrix} 0 & s_1 & 1/c_{55}(x_3) & 0 \\ -s_1 c_{13}(x_3)/c_{33}(x_3) & 0 & 0 & 1/c_{33}(x_3) \\ \rho(x_3) - s_1^2 \zeta(x_3) & 0 & 0 & -s_1 c_{13}(x_3)/c_{33}(x_3) \\ 0 & \rho(x_3) & -s_1 & 0 \end{pmatrix} \begin{pmatrix} \iota\omega\hat{u}_1 \\ \iota\omega\hat{u}_3 \\ \hat{\sigma}_{13} \\ \hat{\sigma}_{33} \end{pmatrix}, \tag{13}$$

with the relations

$$\zeta(x_3) = c_{11}(x_3) - \frac{c_{13}^2(x_3)}{c_{33}(x_3)}, \quad k_1 = \omega s_1, \tag{14}$$

where s_1 is the x_1-component of the slowness. The matrix $\mathbf{Q}$ includes all the information about the heterogeneity of the waveguide because it is expressed from the plate mechanical properties $(\rho(x_3), \mathbb{C}(x_3))$ and from two acoustical parameters (s_1, ω).

2. Explicit solution: The Peano expansion of the matricant

The wave equation thus formulated has an analytical solution expressed between a reference point $(x_1, 0, x_3^0)$ and some point of the plate $(x_1, 0, x_3)$ in the propagation plane. This solution is called the matricant and is explicitly written under the form of the Peano series expansion (Gantmacher, 1959; Peano, 1888; Pease, 1965):

$$\mathbf{M}(x_3, x_3^0) = \mathbf{I} + (\iota\omega)\int_{x_3^0}^{x_3} \mathbf{Q}(\xi)d\xi + (\iota\omega)^2 \times \int_{x_3^0}^{x_3} \mathbf{Q}(\xi)\left(\int_{x_3^0}^{\xi} \mathbf{Q}(\xi_1)d\xi_1\right)d\xi + \ldots, \tag{15}$$

where $\mathbf{I}$ is the identity matrix of dimension (4,4). If the matrix components $\mathbf{Q}(x_3)$ are bounded in the study interval, these series are always convergent (Baron, 2005). The components of the matrix $\mathbf{Q}$ are continuous in x_3 and the study interval is bounded (thickness of the waveguide); consequently the hypothesis is always verified. We underline that the $\iota\omega$-factorization leads up to a polynomial form of the matricant. The $\iota\omega$-polynomial coefficients are matrices independent of ω.

3. Boundary conditions: Fluid-structure interaction

Using the propagator property of the matricant through the plate thickness, the state-vector [defined in Eq. (13)] at the second interface $\eta(d)$ is evaluated from the state-vector at the first interface $\eta(0)$ as follows:

$$\eta(d) = \mathbf{M}(d,0)\,\eta(0). \tag{16}$$

$$\frac{d}{dx_3}\eta(x_3) = \iota\omega\mathbf{Q}(x_3)\,\eta(x_3), \tag{12}$$

that is,

The fluid-structure interaction sets the conditions of zero shear stresses (see Sec. III C), used after a spatio-temporal Fourier transform on (x_1, t). Equation (16) becomes

$$\begin{pmatrix} \iota\omega\hat{u}_1(k_1,d;\omega) \\ \iota\omega\hat{u}_3(k_1,d;\omega) \\ 0 \\ \hat{\sigma}_{33}(k_1,d;\omega) \end{pmatrix} = \begin{pmatrix} M_{11} & M_{12} & M_{13} & M_{14} \\ M_{12} & M_{22} & M_{23} & M_{24} \\ M_{13} & M_{23} & M_{33} & M_{34} \\ M_{14} & M_{24} & M_{34} & M_{44} \end{pmatrix} \times \begin{pmatrix} \iota\omega\hat{u}_1(k_1,0;\omega) \\ \iota\omega\hat{u}_3(k_1,0;\omega) \\ 0 \\ \hat{\sigma}_{33}(k_1,0;\omega) \end{pmatrix}. \tag{17}$$

The condition to obtain a nontrivial solution to Eq. (17) leads to the following relation:

$$\iota\omega\hat{u}_1(k_1,0;\omega) \times M_{13} + \iota\omega\hat{u}_3(k_1,0;\omega) \times M_{32} + \hat{\sigma}_{33}(k_1,0;\omega) \times M_{34} = 0, \tag{18}$$

where M_{ij} (for $i,j = 1,\ldots,4$) represent the components of the matrix $\mathbf{M}$. The displacement component $\hat{u}_1(k_1,0;\omega)$ can be expressed as a linear combination of $\hat{u}_3(k_1,0;\omega)$ and $\hat{\sigma}_{33}(k_1,0;\omega)$; thus system (16) of dimension 4 is reduced to a matrix system of dimension 2

$$\eta(d) = \begin{pmatrix} P_1 & P_2 \\ P_3 & P_4 \end{pmatrix}\eta(0) \quad \text{where} \quad \eta(x_3) = \begin{pmatrix} \iota\omega\hat{u}_3 \\ \hat{\sigma}_{33} \end{pmatrix}, \tag{19}$$

with the relations

$$P_1 = M_{22} - M_{21}\frac{M_{32}}{M_{31}}, \quad P_2 = M_{24} - M_{21}\frac{M_{34}}{M_{31}},$$

$$P_3 = M_{42} - M_{41}\frac{M_{32}}{M_{31}}, \quad P_4 = M_{44} - M_{11}\frac{M_{34}}{M_{31}}. \tag{20}$$

Interface conditions (8) are transformed in the Fourier domain (k_1, ω). The expressions of the displacement and the pressure in the fluids [see Eqs. (3)–(5)], so that the one of the displacement and traction fields in the solid plate [see Eq. (19)], are substituted in the transformed interface conditions.

Setting $\eta(0)=(\alpha_1,\alpha_2)^T \exp \imath(k_1 x_1-\omega t)$, where the superscript ^{T} designates the transpose operator, we obtain the following matrix equation:

$$\begin{pmatrix} \imath\omega s_3^{(1)} c_{f_1} & 1 & 0 & 0 \\ -\imath\omega\rho_{f_1} c_{f_1} & 0 & 1 & 0 \\ 0 & P_1 & P_2 & -\imath\omega s_3^{(2)} c_{f_2} \exp(\imath\omega s_3^{(2)} d) \\ 0 & P_3 & P_4 & -\imath\omega\rho_{f_2} c_{f_2} \exp(\imath\omega s_3^{(2)} d) \end{pmatrix} \begin{pmatrix} \hat{R} \\ \alpha_1 \\ \alpha_2 \\ \hat{T} \end{pmatrix} = \begin{pmatrix} \imath\omega s_3^{(1)} c_{f_1} \\ \imath\omega\rho_{f_1} c_{f_1} \\ 0 \\ 0 \end{pmatrix}, \tag{21}$$

where $\mathbf{s}^{(n)}=\mathbf{k}^{(n)}/\omega$ is the slowness-vector in the fluid f_n ($n=1$ or 2). The quantities $\hat{R}$ and $\hat{T}$ are, respectively, the reflection and transmission coefficients expressed in the Fourier domain: $\hat{R}=\hat{R}(k_1,x_3;\omega)$ and $\hat{T}=\hat{T}(k_1,x_3;\omega)$. The two first lines of system (21) express the boundary conditions at the first interface ($x_3=0$) and the two last lines those at the second interface ($x_3=d$) introducing the Fourier transform of expressions (3)–(5) in the following relations:

$$\eta(0)-\begin{pmatrix} \imath\omega\hat{u}_{3_R}^{(1)} \\ -\hat{p}_R \end{pmatrix}_{x_3=0} = \begin{pmatrix} \imath\omega\hat{u}_{3_I}^{(1)} \\ -\hat{p}_I \end{pmatrix}_{x_3=0},$$

$$\begin{pmatrix} P_1 & P_2 \\ P_3 & P_4 \end{pmatrix} \eta(0)-\begin{pmatrix} \imath\omega\hat{u}_{3_T}^{(2)} \\ -\hat{p}_T \end{pmatrix}_{x_3=d} = \begin{pmatrix} 0 \\ 0 \end{pmatrix}, \tag{22}$$

where $\hat{u}_{3_R}^{(1)}$, $\hat{u}_{3_I}^{(1)}$, and $\hat{u}_{3_T}^{(2)}$ are the components along $\mathbf{x}_3$-axis of $\hat{\mathbf{u}}_R^{(1)}$, $\hat{\mathbf{u}}_I^{(1)}$, and $\hat{\mathbf{u}}_T^{(2)}$ vectors, respectively. Note the equality between the quantities $u_{3_T}^{(2)}$ and $u_3^{(2)}$ where this last is defined in Eq. (9).

4. Expression of the reflection and transmission coefficients

From Eq. (21), we deduce the analytical expressions of the reflection and transmission complex coefficients

$$\hat{R}(s_1,x_3;\omega)=\frac{(P_3-P_1Z_2+P_4Z_1-P_2Z_1Z_2)}{(P_3-P_1Z_2-P_4Z_1+P_2Z_1Z_2)},$$

$$\hat{T}(s_1,x_3;\omega)=-\frac{2Z_2(\rho_{f_1}c_{f_1}/\rho_{f_2}c_{f_2})(P_1P_4-P_2P_3)}{(P_3-P_1Z_2-P_4Z_1+P_2Z_1Z_2)} \times\exp(-\imath\omega s_3^{(2)}d), \tag{23}$$

with $Z_n=\rho_{f_n}/\sqrt{1/c_{f_n}^2-s_1^2}$ (for $n=1$ or 2) and $k_1=\omega s_1$.

IV. VALIDATION OF THE METHOD

The aim of this section is to check that the Peano expansion of the matricant is well-adapted to study fluid-loaded waveguides. We take into account the fluid-structure interaction in different configurations of homogeneous plates comparing the results obtained from the numerical implementation of the Peano expansion of the matricant to results taken from literature.

TABLE I. Elastic properties of transversely isotropic plate (with $c_{23}=c_{22}-2c_{44}$).

ρ (g cm^{-3})	c_{11} (GPa)	$c_{22}=c_{33}$ (GPa)	$c_{12}=c_{13}$ (GPa)	c_{44} (GPa)	$c_{66}=c_{55}$ (GPa)
1.85	23.05	15.1	8.7	3.25	4.7

The numerical evaluation of P_1, P_2, P_3, and P_4 requires us to truncate the Peano series and to numerically calculate the integrals. Thus, the error can be estimated and controlled (Baron, 2005). We retained 70 terms in the series and evaluate the integrals over 100 points using Simpson's rule (fourth-order integration method). These choices ensure the convergence of the solution and the accuracy of the results for a reasonable computation-time (never exceeding few minutes on a desktop computer). Expressions (23) give the frequency spectrum (modulus and phase) of the reflection coefficient for different incidences (s_1 varies from zero-normal incidence to $1/c_{f_1}$ corresponding to the critical incidence in the fluid f_1).

A lot of works detailed the relationship between the poles and the zeros of the reflection coefficient and the leaky Lamb wave dispersion curves (Chimenti and Rokhlin, 1990; Deschamps and Poncelet, 2000). The results of Sec. IV A compare the dispersion curves obtained by seeking the poles of reflection coefficient (23) and the results taken from literature or from closed-form solution.

A. Validation for a homogeneous and isotropic or anisotropic fluid-loaded plate

The method is tested by plotting the dispersion curves (variation of the phase velocity versus frequency-thickness product) for an isotropic aluminum plate immersed in water. The data in the paper of Chimenti and Rokhlin (1990) are used. The results obtained (not shown) by the present method are in perfect agreement with the results presented by them (Chimenti and Rokhlin, 1990).

As mentioned by Chimenti and Rokhlin (1990), there are few differences between the zeros' loci and the poles' loci for a plate immersed in a fluid whose the mass density is lower than the plate mass density. As underlined by several authors, fluid-load does have just a weak influence on guided wave traveling in the plate immersed in water.

Taking into account the anisotropy does not change the scheme for the numerical solution of wave equation with the matricant. We consider a transverse isotropic plate immersed in water ($\rho_f=1$ g cm^{-3}, $c_f=1.485$ mm μs^{-1}) whose properties are reported in Table I. For that configuration, Nayfeh and Chimenti (1989) developed a method to obtain an analytical expression of the reflection coefficient. By using the data from this paper, the results obtained (see Fig. 1) with the present method are in perfect agreement with theirs. The curves presented in Figs. 1(a) and 1(b) are superimposed and need to be presented separately.

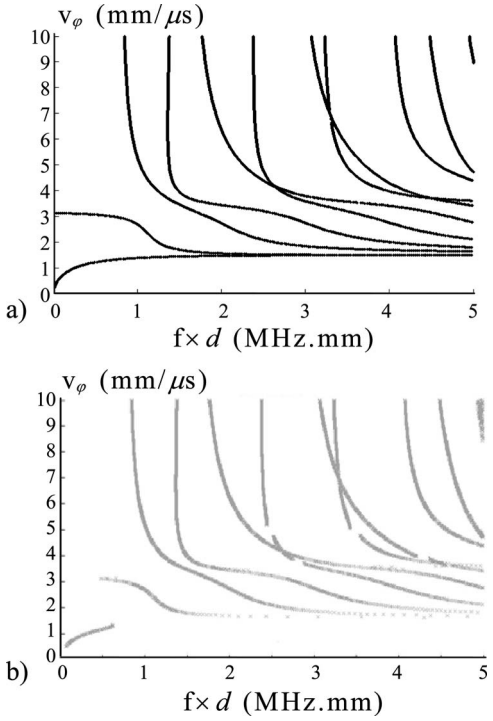

FIG. 1. Dispersion curves for a transversely isotropic plate immersed in water; comparison between (a) analytical results from Nayfeh and Chimenti (1989) and (b) results obtained via the Peano series of the matricant.

B. Validation for an asymmetrically loaded homogeneous isotropic plate ($f_1 \neq f_2$)

The formalism presented here to solve the wave equation in an unidirectionally graded medium presents two main advantages: Without changing the scheme to obtain the numerical solution we can take into account (i) an asymmetric loading and (ii) the unidirectional continuous heterogeneity.

The mechanical behavior of the plate is different for symmetric and asymmetric loadings. For example, in the symmetric loading case, there is a unique critical frequency and a unique phase velocity value v_φ in the plate, which corresponds to the propagation velocity in the fluid ($v_\varphi = c_{f_1} = c_{f_2}$), for which the displacements and the stresses at the interfaces are quasi-null; whereas in the asymmetric loading ($f_1 = f_2$), there are two critical frequencies and two values of the phase velocity in the plate for which the structure does not respond (Dickey *et al.*, 1995). The validation is done on an isotropic aluminum plate with the following properties: $\rho = 2.79$ g cm^{-3}; the longitudinal and transverse wave velocities are, respectively, $v_L = 6.38$ mm μs^{-1} and $v_T = 3.10$ mm μs^{-1}. The characteristic properties of the fluid f_1 correspond to those of water (see Sec. IV A); the characteristic properties of the fluid f_2 correspond to glycerine: $\rho_{f_2} = 1.26$ g cm^{-3} and $c_{f_2} = 1.920$ mm μs^{-1}. This configuration is the same as the one studied by Franklin *et al.* (2001). The modulus of the reflection coefficient versus the incident angle is plotted in Fig. 2 for a fixed frequency-thickness product ($f \times d = 4.7$ MHz mm).

This figure shows the perfect agreement between our results and the ones presented by Franklin *et al.* (2001).

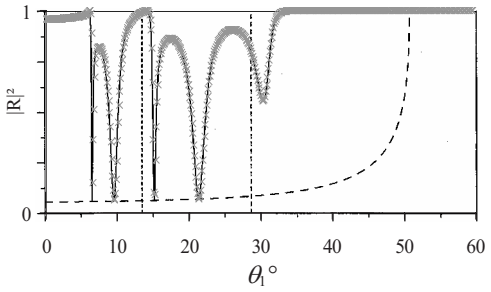

FIG. 2. Reflection coefficient modulus for an asymmetrically fluid-loaded aluminum plate (water and glycerine) versus incident angle: in dark lines results published in Franklin *et al.* (2001), and in gray crosses the reflection coefficient modulus calculated from Eq. (23). The vertical lines (dashed) represent the two critical angles for longitudinal waves and transverse waves. The dashed curve corresponds to the resonant amplitudes (Franklin *et al.*, 2001).

V. RELEVANCY OF THE METHOD FOR ULTRASOUND CHARACTERIZATION OF CORTICAL BONE

Cortical bone is a kind of hard tissue found at the edges of long bones and supports most of the load of the body. Several studies demonstrated the heterogeneous nature of the cortical bone, particularly they show evidence the gradual variation of the volumetric porosity (ratio between pores and total volume) along the cortical thickness. Yet, the porosity is intrinsically linked to the macroscopic mechanical behavior of the cortical bone (Baron *et al.*, 2007). Therefore, the continuous variation of porosity induces a continuous variation of material properties. Taking into account the gradient should prove itself to be essential in the context of diagnosis and therapeutic monitoring of osteoporosis. Indeed, the gradient characterization would allow assessing geometrical (cortex thickness) and material (elastic coefficients variation) information, which are fundamental parameters to evaluate the bone fragility. For several years, the quantitative ultrasonography (by axial and transverse transmissions) proved itself to be a hopeful alternative technique to evaluate the fracture risk (Marin *et al.*, 2006). However, the inter-individual and inter-site variations of bone mechanical properties make the standardization of the protocol of fracture risk evaluation by ultrasound very delicate.

The focus is set on a configuration closed to the axial transmission device for *in vivo* conditions. In this context, the relevancy of studying the head wave propagation has been demonstrated (Bossy *et al.*, 2004a, 2004b; Camus *et al.*, 2000). As a consequence all the reflection coefficients presented in this paper were calculated for an incident angle corresponding to the grazing-angle for longitudinal waves [critical angle of longitudinal wave propagation in the plate at the first interface ($x_3 = 0$)].

The surrounding media in the *in vivo* configuration of ultrasound characterization of cortical bone are the muscle for the upper fluid f_1 ($c_{f_1} = 1.54$ mm μs^{-1} and $\rho_{f_1} = 1.07$ g cm^{-3}) and the marrow for the lower fluid f_2 ($c_{f_2} = 1.45$ mm μs^{-1} and $\rho_{f_2} = 0.9$ g cm^{-3}) (Burlew *et al.*, 1980; Hill *et al.*, 1986). We are interested in the influence of the continuous gradient of the mechanical properties on the ultrasonic response in the configuration of *in vivo* cortical bone characterization.

A. Determination of a realistic range of variation of elastic bone properties

In order to define numerical values for a realistic value of the gradient of the different material properties, it is necessary to determine the limiting values reached by each elastic property. Our approach consists in considering *in vitro* measurements published in Dong and Guo, 2004 and performed in 18 samples. It is assumed that these limiting values for elastic properties are relevant for physiologic ranges of variations.

We assume that cortical bone is transverse isotropic. Transverse isotropy has been shown experimentally by different authors (Dong and Guo, 2004; Reilly and Burnstein, 1974; Rho, 1996) to be a realistic approximation of cortical bone degree of anisotropy.

Dong and Guo (2004) measured the homogenized bone properties by performing tensile and torsional tests with a mechanical testing system on 18 different human femoral bone specimens. The authors measured the values of the longitudinal and transverse Young's moduli (E_L and E_T, respectively) as well as the values of the longitudinal shear modulus G_L. From these measurements and by assuming constant values of Poisson's ratio, the values of the different components of the stiffness-tensor corresponding to the values of E_L, E_T, and G_L measured in Dong and Guo, 2004 were obtained following the relationships given in the Appendix.

The value of the longitudinal Poisson's ratio ν_L is taken equal to 0.37 for all computations because it corresponds to the average value found in Dong and Guo, 2004. The value of the transverse Poisson's ratio ν_T is taken equal to 0.45 following Eq. (A3) of the Appendix. The values of the stiffness coefficients corresponding to the mean values of the bone mechanical properties are referred to as "reference" set of parameters in what follows. The maximum and minimum values of the stiffness coefficients are obtained by considering, respectively, the maximum and minimum values of E_L and E_T within the range of variation measured in Dong and Guo, 2004, which is a simple way to obtain a realistic range of variation for the stiffness coefficients in cortical bone. Furthermore, the elastic properties deduced from the approach reported above were constrained to verify the thermodynamical stability conditions given in the Appendix by Eq. (A4).

We choose reference value of mass density ρ equal to 1.722 g cm^{-3}, following the value taken in Macocco *et al.*, 2006. In order to derive a realistic range of variation for mass density, we assume that the reference value is given by a porosity of 7%, which corresponds approximately to the mean porosity at the radius (Baron *et al.*, 2007). The porosity was assumed to vary between 3% and 15% (Bousson *et al.*, 2001; Dong and Guo, 2004) and a rule of mixture leads to the range of variation of mass density.

B. Modeling a gradient of material property

The impact of a controlled gradient vector $\boldsymbol{\delta}$ of any investigated material property S on the response of the structure studied is assessed. The scalar S corresponds to one of the stiffness coefficients c_{ij} of $\mathbb{C}$ or to mass density ρ. In each set of simulations, all the material properties are constant and equal to their reference value while S is subjected to the defined gradient.

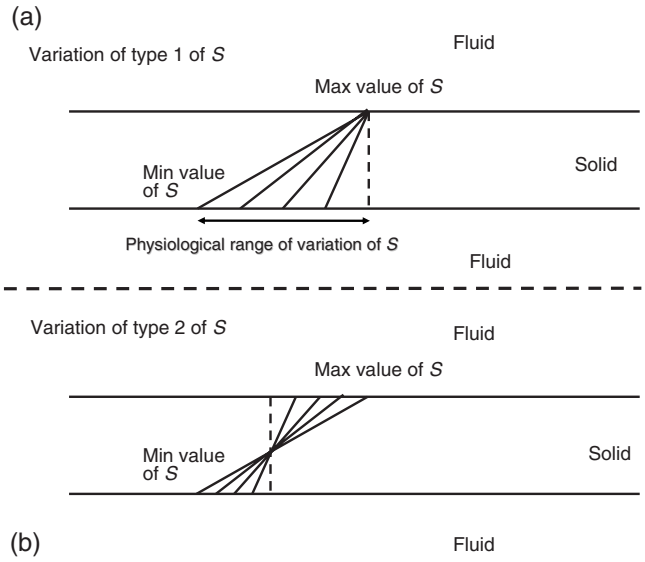

FIG. 3. Schematic representation of the two types of spatial variation considered for the material property S corresponding to the stiffness coefficient and to mass density. The solid lines in the solid layer indicate the spatial dependence of S. The dotted line in the solid layer indicates homogeneous material properties corresponding to the reference material properties. The variation of type 1 shown in (a) corresponds to a constant value at the bone-soft tissues' interface. The variation of type 2 shown in (b) corresponds to a constant value in the middle of the bone.

The gradient vector $\boldsymbol{\delta}=\text{grad}\, S=\delta \mathbf{x}_3$ is assumed to be independent of x_1 in all cases, where $\mathbf{x}_3$ is a unit vector along $\mathbf{x}_3$-axis and grad is the gradient operator acting on a scalar field. The quantity δ is always taken positive because the porosity is known to be higher in the endosteal part ($x_3=d$) than in the periosteal part ($x_3=0$) of the bone. Moreover, only the simple situation of affine spatial variations of S is considered, corresponding to a constant value of δ. This affine spatial variation of S is chosen because the actual physiological spatial dependence of S remains unknown. Two different affine spatial dependencies of the studied material property are considered and are illustrated in Fig. 3. Associated gradient δ will be referred to as type 1 or 2.

Type 1. The gradient of type 1 is such that the physical property S takes the same value S_M at the upper interface $x_3=0$ of the solid plate for all values of the gradient δ. The quantity $S(x_3)$ is therefore given by

$$S(x_3) = S_M + \delta \times x_3, \tag{24}$$

where S_M is given by the maximal value of the material property S considered. The maximal value δ_M of δ is chosen so that $S(d)$ is equal to S_m, where S_m is given by the minimal value of S. The gradient δ_M is given by

$$\delta_M = \frac{(S_m - S_M)}{d}. \tag{25}$$

Type 2. The gradient of type 2 is such that the physical property S takes the same value at the middle $x_3=d/2$ of the solid plate for all values of gradient δ. Furthermore, the

TABLE II. Mean value, maximum, and minimum values of the homogenized longitudinal and transversal Young moduli, of the four elastic constants and of mass density affecting the ultrasonic propagation in the framework of the model. These values are taken from Dong and Guo (2004).

Mechanical quantity	E_L (GPa)	E_T (GPa)	c_{11} (GPa)	c_{13} (GPa)	c_{33} (GPa)	$c_{55}=G_L$ (GPa)	ρ (g cm^{-3})
Mean value (reference)	16.6	9.5	23.1	8.7	15.1	4.7	1.722
Minimum	13.4	6.5	17.6	5.1	9.1	3.3	1.66
Maximum	20.6	12.8	29.6	15.9	25.9	5.5	1.753

mean value of the property S is identical for all δ. The quantity $S(x_3)$ is given by

$$S(x_3) = \frac{(S_m + S_M)}{2} + \delta \times \left(x_3 - \frac{d}{2} \right). \tag{26}$$

The maximal value of δ is also given by Eq. (25), so that all values of $S(x_3)$ are again always comprised between S_m and S_M. Again, the maximal value δ_M of δ is given by Eq. (25).

Gradient of type 2 leads for all magnitudes of δ to a constant value of the spatial average of the gradient.

For both types of spatial variations, five different values of δ regularly distributed between 0 and δ_M are arbitrarily considered in the thickness.

Table II recalls the maximum, minimum, and mean measured values of E_L, E_T, and G_L as given by Dong and Guo (2004). Table II also shows the maximum, minimum, and mean values of the four components (c_{11}, c_{13}, c_{33}, and c_{55}) of the stiffness-tensor $\mathbb{C}$ affecting wave propagation derived from Eq. (A3) of the Appendix.

In Table III, the minimal and maximal values of each variable corresponding to the realistic range of variation obtained (i) by considering the reference values of Table II and (ii) by verifying that the thermodynamical stability conditions are fulfilled. Values resulting from the stability conditions are marked with an asterisk.

In the simulations, the values of S_M and S_m are those reported in Table III.

C. Results and discussion

First of all, the method allows investigating the influence of the fluids on the ultrasonic response. In the case of the characterization of cortical bone, the two fluids f_1 and f_2 are different, which corresponds to an asymmetrical loading (see Sec. IV B): The fluid f_1 has been considered as muscle ($c_{f_1}=1540$ m s^{-1} and $\rho_{f_1}=1.07$ g cm^{-3}) and fluid f_2 as marrow ($c_{f_2}=1450$ m s^{-1} and $\rho_{f_2}=0.9$ g cm^{-3}). The properties of these two fluids are very close to those of water. The frequency spectrum of the reflection coefficient modulus has been plotted for the *in vivo* configuration and compared with the result obtained for a cortical bone plate immersed in water for the ten profiles of mechanical properties (figure not shown). For homogeneous plates as for linearly graded plates, the two curves are very close; however, the modulus of the reflection coefficient at null-frequency is not null and the minimum values are greater than for water but obtained for the same frequency-thickness products. That is why all the following results have been calculated for a cortical bone plate immersed in water.

The reflection coefficient calculated with the Peano series of the matricant is sensitive to the variation of the properties gradient. As we consider that the osteoporosis entails a trabecularization of cortical bone from the endosteal side, the characterization of the gradient of the properties between the endosteal and periosteal regions may be an element of the diagnosis of the osteoporosis progress and of the therapeutic follow-up.

It is known that the gradient of the properties along the cortical thickness is due to the continuous variation of the porosity growing progressively from the periosteal to the endosteal region. From previous work, we know that the porosity influences all the stiffness coefficients (Baron *et al.*, 2007). The frequency spectrum of the reflection coefficient has been plotted for the ten profiles presented in Fig. 3 applied to all the stiffness coefficients implied (c_{11}, c_{13}, c_{33}, and c_{55} and to the mass density ρ) (see Table III). The reflection coefficients have been calculated at an incident angle corresponding to the grazing-angle (critical angle for the longitudinal waves in the bone plate). For the two types of gradients, differences appear between all the gradients and the homogenized plates (corresponding to the maximum value for type 1 and to the average value for type 2) particularly on the location of the extrema values of the reflection coefficient modulus (see Fig. 4).

The increase in the gradient of properties shifts the minimum and maximum values forward high frequency-thickness products. However, the results (see Fig. 4) put on evidence that the behavior of the reflection coefficient modulus is sensibly the same for frequency-thickness products be-

TABLE III. The minimal and maximal values of each variable corresponding to the realistic range of variation obtained (i) by considering the reference values of Table II and (ii) by verifying that the thermodynamical stability conditions are fulfilled. Values resulting from the stability conditions are marked with an asterisk.

Material property S	c_{11} (GPa)	c_{13} (GPa)	c_{33} (GPa)	$c_{55}=G_L$ (GPa)	ρ (g cm^{-3})
Realistic range $[S_m, S_M]$ (reference)	[17.6, 29.6]	[5.1, 11.1*]	[11.8*, 25.9]	[3.3, 5.5]	[1.66, 1.753]

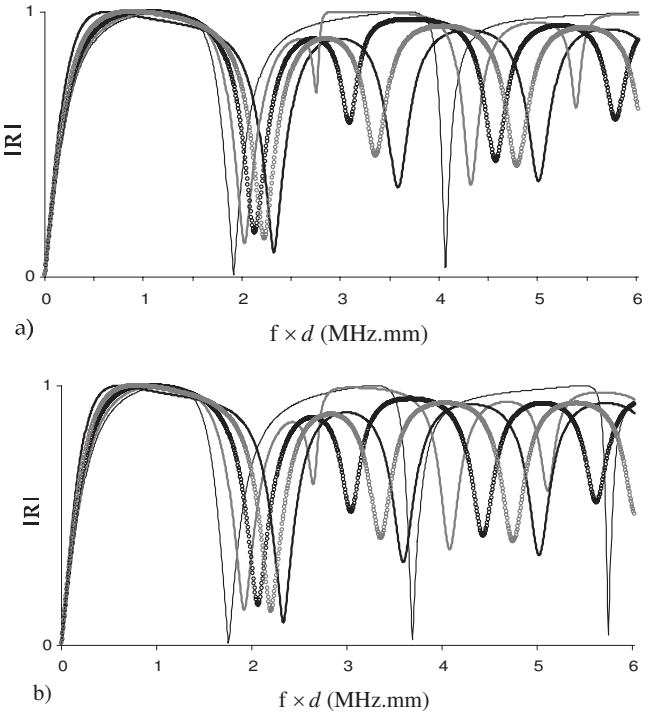

FIG. 4. Frequency spectrum of the reflection coefficient modulus for different properties' variations corresponding to (a) the five profiles of type 1 [Fig. 3(a)] and (b) the five profiles of type 2 [Fig. 3(b)].

tween 0 and 1.5 MHz mm. Beyond this value, the behavior is clearly different. At sufficiently high frequency, the wavelength is smaller and more sensitive to the affine variation of the material properties. It is noteworthy that for a heterogeneous waveguide, the minima of the reflection coefficient magnitude do not reach zero (except for null-frequency) but end at a finite value and the changes in phase (not shown) are not so rapid, which means that total transmission does not take place in this situation.

The influence of the variation of each parameter (stiffness coefficients) on the frequency spectrum of the reflection coefficient has been investigated. This analysis has been led for an incidence angle corresponding to the longitudinal wave critical angle in the plate at $x_3=0$. This incidence corresponds to the generation and the propagation of the head wave.

It appears that each of them has an impact on the reflection wave, but the leading term is c_{11}. The frequency spectrum of the reflection coefficient for a varying c_{11} in an affine way is very close to the frequency spectrum of the reflection coefficient obtained for the affine variation of all the material properties (c_{ij} and ρ) and is the most different to the results from homogenized plates (average value or maximum value) compared to the frequency spectrum calculated for the *one-parameter variation* of the other elastic parameters (c_{13}, c_{33}, and c_{55}, and ρ) (see Fig. 5). It is noteworthy that c_{11} is the stiffness coefficient associated with the axial direction and determining the speed of the head wave. So, it seems that the head wave would be the indicator of the c_{11} gradient. It is important to note that for homogenized plates (extremum value or average) the frequency spectrum of the reflection coefficient is really different from that of the plate with continuously varying properties. We infer that the approximation by a homogeneous plate of cortical bone and all the more so for the osteoporotic cortical bone (for which the gradient would be greater) may induce bad interpretation of the ultrasonic response.

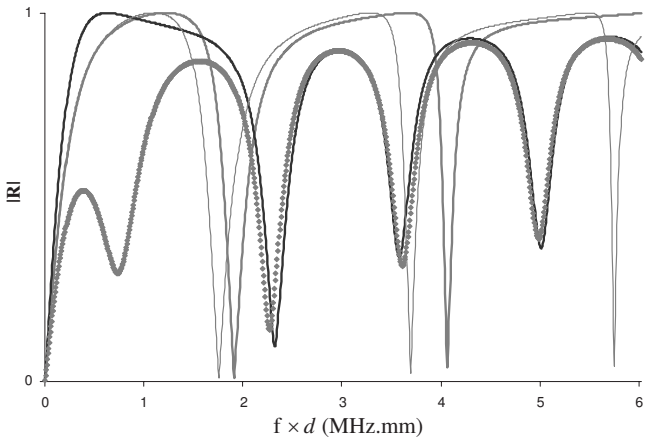

FIG. 5. Frequency spectrum of the reflection coefficient modulus for different properties' variations at grazing-incidence $\theta_1=\theta_c$: for a homogeneous plate whose properties are those at $x_3=0$ at $\theta_c=21.1°$ (thick gray line), for a homogeneous plate whose properties are the average of the properties through the plate at $\theta_c=23.6°$ (thin gray line), for a plate with all its properties linearly varying at $\theta_c=21.1°$ (black line), and for a plate with an affine variation of the c_11 only at $\theta_c=21.1°$ (gray lozenges).

The authors do not know any results in literature about the measurement of the variation of the porosity within the cortical thickness. The assumption of an affine gradient is a first step; other gradients may be investigated and the method presented in this article would be applied in the same way for non-affine gradients (Shuvalov *et al.*, 2005).

VI. CONCLUSION AND PERSPECTIVES

Stroh's (1962) sextic plate formalism has been employed for analyzing the leaky Lamb waves in anisotropic heterogeneous plates immersed in fluids. This formalism and especially the polynomial form of the solution [see Eq. (15)] presents several analytical and numerical advantages. First, the low-frequency asymptotics are naturally assessed evaluating only two or three terms in the series (Shuvalov *et al.*, 2005). The information thus collected is of major interest in the analysis of the elastic behavior of waveguides (Baron *et al.*, 2008). Second, the polynomial form makes the numerical evaluation of the solution faster. Indeed, the polynomial coefficients are independent of the frequency, so they are calculated for a fixed slowness value and stored. When the frequency varies, there is no need to recalculate the polynomial coefficients, it comes to a polynomial evaluation whose coefficients are perfectly known, which is time-saving.

The Peano series of the matricant is a method that keeps the continuity of the profiles and so, the authenticity of the problem. One of the key points for methods based on multilayered media to deal with FGM is to relevantly discretize the properties' profiles. The choice of the discretization may lead to some errors especially in the evaluation of the resonances.

This elegant mathematical tool is also very adaptative to different physical problems. In the case studied—a fluid-loaded plane waveguide—the anisotropy, the heterogeneity (continuous or discontinuous variation of properties) and the asymmetric fluid-loading are taken into account without changing the resolution scheme.

Further work needs to be done to relate the results presented in this paper to dispersion curves and propagation of transient and heterogeneous waves in a fluid-loaded continuously heterogeneous waveguide.

Furthermore, from this study, the transient response of a fluid-loaded plate is considered. The frequency spectrum of the reflection coefficient is calculated for incidences between the normal and critical incidences for compression waves in the fluid f_1. Thus, the plate transfer function is calculated in the Fourier domain (x_1-wavenumber, frequency): $\hat{R}(k_1,x_3;\omega)$. A double inverse Fourier transform on (k_1,ω) is applied on $\hat{R}(k_1,x_3;\omega)$ to transform into the space-time domain; the temporal signals can be obtained at different points along the propagation $\mathbf{x}_3$-axis: $R(x_1,x_3;t)$.

Lastly, the formalism presented here is well-adapted to deal with wave propagation in anisotropic tubes with radial property gradients (Shuvalov, 2003). The wave equation keeps the same form as Eq. (12), the state-vector is expressed from the displacement and traction components in the cylindrical basis, and the matrix $\mathbf{Q}$ depends on the radial position r ($\mathbf{Q}=\mathbf{Q}(r)$). In cylindrical homogeneous structures, taking into account an anisotropy more important than transverse isotropy is fussy because there is no analytical solution to the "classical" wave equation (second-order differential equation). Stroh's (1962) formalism, upon which the Peano expansion of the matricant is based, is a promising alternative solution that allows considering altogether the geometry (cylinder), the anisotropy, and the heterogeneity (radial property gradients) of a structure.

APPENDIX: THERMODYNAMICS STABILITY CONDITIONS AND STIFFNESS COEFFICIENTS

Hooke's law is written under the form $\sigma_{ij}=C_{ijk\ell}\epsilon_{k\ell}$ for $(i,j,k,\ell=1,\ldots,3)$, where σ is the stress-tensor, ϵ is the strain-tensor, and $\mathbb{C}$ is the fourth-order stiffness-tensor. In the transversely isotropic case, with $(\mathbf{x}_2,\mathbf{x}_3)$ as isotropic plane, the stiffness-tensor is expressed as a stiffness matrix (using Voigt's notation)

$$\mathbb{C}=\begin{pmatrix} c_{11} & c_{13} & c_{13} & 0 & 0 & 0 \\ c_{13} & c_{33} & c_{23} & 0 & 0 & 0 \\ c_{13} & c_{23} & c_{33} & 0 & 0 & 0 \\ 0 & 0 & 0 & c_{44} & 0 & 0 \\ 0 & 0 & 0 & 0 & c_{55} & 0 \\ 0 & 0 & 0 & 0 & 0 & c_{55} \end{pmatrix}. \tag{A1}$$

We introduce the matrix $\mathbb{S}$, the inverse of the matrix $\mathbb{C}$. It is expressed by

$$\mathbb{S}=\begin{pmatrix} 1/E_L & -\nu_L/E_L & -\nu_L/E_L & 0 & 0 & 0 \\ -\nu_L/E_L & 1/E_T & -\nu_T/E_T & 0 & 0 & 0 \\ -\nu_L/E_L & -\nu_T/E_T & 1/E_L & 0 & 0 & 0 \\ 0 & 0 & 0 & 1/G_T & 0 & 0 \\ 0 & 0 & 0 & 0 & 1/G_L & 0 \\ 0 & 0 & 0 & 0 & 0 & 1/G_L \end{pmatrix}. \tag{A2}$$

with $E_{L,T}$, the longitudinal (L) and transverse (T) Young's moduli; $\nu_{L,T}$, the longitudinal (L) and transverse (T) Poisson's ratios; and $G_{L,T}$, the longitudinal (L) and transverse (T) shear moduli. By inverting Eq. (A1)and identifying it with Eq. (A2), we obtain the following relations:

$$E_L=\frac{c_{11}c_{33}-2c_{13}^2+c_{11}c_{23}}{c_{33}+c_{23}}, \quad \nu_L=\frac{c_{13}}{c_{33}+c_{23}},$$

$$E_T=\frac{c_{11}(c_{33}^2-c_{23}^2)+2c_{13}^2(c_{23}-c_{33})}{c_{11}c_{33}-c_{13}^2}, \quad \nu_T=\frac{c_{11}c_{23}-c_{13}^2}{c_{11}c_{33}-c_{13}^2},$$

$$G_T=c_{44}, \quad G_L=c_{55}. \tag{A3}$$

Knowing the stiffness coefficient values, we can verify if the thermodynamical stability conditions are satisfied as follows:

$$E_L>0, \quad E_T>0, \quad -1<\nu_T<1,$$

$$\frac{(1-\nu_T)}{2}\frac{E_L}{E_T}-\nu_L^2>0, \quad G_L>0. \tag{A4}$$

Baron, C. (**2005**). "Peano expansion of the matricant to study elastic wave propagation in continuously heterogeneous media," University Bordeaux 1 (in French).

Baron, C., Poncelet, O., Shuvalov, A., and Deschamps, M. (**2008**). "Propagation in continuous stratification environment," in *Materials and Acoustics Handbook*, edited by M. Bruneau and C. Potel (ISTE Ltd. and Wiley, London, UK), Chap. 6.

Baron, C., Talmant, M., and Laugier, P. (**2007**). "Effect of porosity on effective diagonal stiffness coefficients (c_{ii}) and anisotropy of cortical at 1 MHz: A finite-difference time domain study," J. Acoust. Soc. Am. **122**, 1810–1817.

Bossy, E., Talmant, M., and Laugier, P. (**2004a**). "Three-dimensional simulations of ultrasonic axial transmission velocity measurement on cortical bone models," J. Acoust. Soc. Am. **115**, 2314–2324.

Bossy, E., Talmant, M., Peyrin, F., Akrout, L., Cloetens, P., and Laugier, P. (**2004b**). "An *in vitro* study of the ultrasonic axial transmission technique at the radius: 1-MHz velocity measurements are sensitive to both mineralization and intracortical porosity," J. Bone Miner. Res. **19**, 1548–1556.

Bousson, V., Meunier, A., Bergot, C., Vicaut, E., Rocha, M. A., Morais, M. H., Laval-Jeantet, A. M., and Laredo, J. D. (**2001**). "Distribution of intracortical porosity in human midfemoral cortex by age and gender," J. Bone Miner. Res. **16**, 1308–1317.

Brekhovskikh, L. M. (**1980**). *Waves in Layered Media* (Academic, New York).

Burlew, M., Madsen, E., Zagzebski, J., Banjavic, R., and Sum, S. (**1980**). "A new ultrasound tissue-equivalent material," Radiology **134**, 517–520.

Camus, E., Talmant, M., Berger, G., and Laugier, P. (**2000**). "Analysis of the axial transmission technique for the assessment of skeletal status," J. Acoust. Soc. Am. **108**, 3058–3065.

Chimenti, D. E., and Nayfeh, A. H. (**1986**). "Anomalous ultrasonic dispersion in fluid-coupled, fibrous composite plates," Appl. Phys. Lett. **49**, 492–493.

Chimenti, D. E., and Nayfeh, A. H. (**1990**). "Ultrasonic reflection and guided waves in fluid-coupled composite laminates," J. Nondestruct. Eval. **9**, 51–69.
Chimenti, D. E., and Rokhlin, S. (**1990**). "Relationship between leaky Lamb modes and reflection coefficient zeroes for a fluid-coupled elastic layer," J. Acoust. Soc. Am. **88**, 1603–1611.
Deschamps, M., and Poncelet, O. (**2000**). "Transient Lamb waves: Comparison between theory and experiment," J. Acoust. Soc. Am. **107**, 3120–3129.
Dickey, J., Maidanik, G., and Uberall, H. (**1995**). "The splitting of dispersion curves for the fluid-loaded plate," J. Acoust. Soc. Am. **98**, 2365–2367.
Dong, X. N., and Guo, X. E. (**2004**). "The dependence of transversely isotropic elasticity of human femoral cortical bone on porosity," J. Biomech. **37**, 1281–1287.
Fiorito, R., Madigosky, W., and Überall, H. (**1979**). "Resonance theory of acoustic waves interacting with an elastic plate," J. Acoust. Soc. Am. **66**, 1857–1866.
Folds, D. L., and Loggins, C. D. (**1977**). "Transmission and reflection of ultrasonic waves in layered media," J. Acoust. Soc. Am. **62**, 1102–1109.
Franklin, H., Danila, E., and Conoir, J.-M. (**2001**). "S-matrix theory applied to acoustic scattering by asymmetrically fluid-loaded elastic isotropic plates," J. Acoust. Soc. Am. **110**, 243–253.
Gantmacher, F. (**1959**). *The Theory of Matrices* (Wiley, New York).
Haskell, N. A. (**1953**). "The dispersion of surface waves on multilayered media," Bull. Seismol. Soc. Am. **43**, 377–393.
Hill, C., Bamber, J., and Ter Haar, G. (**1986**). *Physical Principles of Medical Ultrasonics* (Wiley, New York).
Hosten, B., and Castaings, M. (**2003**). "Surface impedance matrices to model the propagation in multilayered media," Ultrasonics **41**, 501–507.
Kenneth, E. G. (**1982**). "A propagator matrix method for periodically stratified media," J. Acoust. Soc. Am. **73**, 137–142.
Lamb, H. (**1917**). "On waves in an elastic plate," Proc. R. Soc. London Ser. A **93**, 114–128.
Lévesque, D., and Piché, L. (**1992**). "A robust transfer matrix simulation for ultrasonic response of multilayered absorbing media," J. Acoust. Soc. Am. **92**, 452–467.
Macocco, K., Grimal, Q., Naili, S., and Soize, C. (**2006**). "Elastoacoustic model with uncertain mechanical properties for ultrasonic wave velocity prediction; application to cortical bone evaluation," J. Acoust. Soc. Am. **119**, 729–740.
Marin, F., Gonzales-Macias, J., Diez-Perez, A., Palma, S., and Delgado-Rodriguez, M. (**2006**). "Relationship between bone quantitative ultrasound and fractures: A meta-analysis," J. Bone Miner. Res. **21**, 1126–1135.
Nayfeh, A. H., and Chimenti, D. E. (**1988**). "Ultrasonic wave reflection from liquid-coupled orthotropic plates with application to fibrous composites," ASME J. Appl. Mech. **55**, 863–870.
Nayfeh, A. H., and Chimenti, D. E. (**1989**). "Free wave propagation in plates of general anisotropic media," ASME J. Appl. Mech. **56**, 881–886.
Peano, G. (**1888**). "Integration by series of linear differential equations (in French)," Math. Ann. **32**, 450–456.
Pease, M. (**1965**). *Methods of Matrix Algebra* (Academic, New York).
Pitts, L. E., Plona, T. J., and Mayer, W. G. (**1976**). "Theoretical similarities of Rayleigh and Lamb modes of vibration," J. Acoust. Soc. Am. **60**, 374–377.
Rayleigh, J. W. S. (**1885**). "On wave propagating along the plane surface of an elastic solid," Proc. London Math. Soc. **s1-17**, 4–11.
Reilly, D. T., and Burnstein, A. H. (**1974**). "The mechanical properties of cortical bone," J. Bone Jt. Surg., Am. Vol. **56**, 1001–1022.
Rho, J. Y. (**1996**). "An ultrasonic method for measuring the elastic properties of human tibial cortical and cancellous bone," Ultrasonics **34**, 777–783.
Rokhlin, S. I., and Wang, L. (**2002**). "Stable recursive algorithm for elastic wave propagation in layered anisotropic media: Stiffness matrix method," J. Acoust. Soc. Am. **112**, 822–834.
Rose, J. L. (**2002**). "A baseline and vision of ultrasonic guided wave inspection potential," J. Pressure Vessel Technol. **124**, 273–282.
Shuvalov, A. (**2003**). "A sextic formalism for three-dimensional elastodynamics of cylindrically anisotropic radially inhomogeneous materials," Proc. R. Soc. London, Ser. A **459**, 1611–1639.
Shuvalov, A., Poncelet, O., Deschamps, M., and Baron, C. (**2005**). "Long-wavelength dispersion of acoustic waves in transversely inhomogeneous anisotropic plates," Wave Motion **42**, 367–382.
Stroh, A. N. (**1962**). "Steady state problems in anisotropic elasticity," J. Math. Phys. **41**, 77–103.
Thomson, W. T. (**1950**). "Transmission of elastic waves through a stratified solid medium," J. Appl. Phys. **21**, 89–93.
Vlasie, V., and Rousseau, M. (**2004**). "Guided modes in a plane elastic layer with gradually continuous acoustic properties," NDT & E Int. **37**, 633–644.
Wang, L., and Rokhlin, S. I. (**2001**). "Stable reformulation of transfer matrix method for wave propagation in layered anisotropic media," Ultrasonics **39**, 413–424.
Worlton, H. (**1961**). "Experimental confirmation of Lamb waves at megacycle frequencies," J. Appl. Phys. **32**, 967–971.
Youssef, I., and El-Arabawi, H. (**2007**). "Picard iteration algorithm combined with Gauss-Seidel technique for initial value problems," Appl. Math. Comput. **190**, 345–355.